CrystEngComm

ROYAL SOCIETY OF CHEMISTRY

COMMUNICATION

View Article Online
View Journal | View Issue

Cite this: *CrystEngComm*, 2020, **22**, 5941

Received 1st June 2020,
Accepted 14th July 2020

DOI: 10.1039/d0ce00798f

rsc.li/crystengcomm

Structural tuning of Zn(II)-MOFs based on pyrazole functionalized carboxylic acid ligands for organic dye adsorption†

Xiao-Ting Liu,‡[ab] Si-Si Chen,‡[a] Si-Miao Li,[a] Hong-Xiang Nie,[ab] Yao-Qing Feng,[a] Yi-Ning Fan,[a] Mei-Hui Yu, *[ab] Ze Chang *[abc] and Xian-He Bu [abd]

Two metal–organic frameworks, $\{(NH_2Me_2)[Zn(Pycia)]\}_n$ (MOF-1) and $\{(NH_2Me_2)[Zn_2(Pycia)(PBA)]\}_n$ (MOF-2), have been synthesized based on pyrazole functionalized carboxylic acid ligands for organic dye adsorption. The enlarged pore dimension of MOF-2 suggests the advantage of additional linear auxiliary ligand for the structure tuning of the MOFs. Furthermore, the anionic frameworks of the MOFs endow them with size selective adsorption toward different cationic organic dyes.

Organic dyes are critical compounds for industrial applications such as textile, printing, leather, *etc.*[1] However, they could also induce serious threats to the environment and human health.[2,3] Due to the stability of the dye molecules, their degradation and elimination under natural conditions can be difficult.[4] As an alternative approach, the physical adsorption of dyes with porous materials could be a straightforward and effective way.

In this context, metal–organic frameworks (MOFs), as a class of newly-developed materials with high porosity and designable channels,[5–7] have caught much attention. As a new class of porous materials constructed from metal ions or clusters and organic ligands through coordination bonds,[8–10] MOFs feature highly tuneable structures and adsorption properties, which make them widely investigated in storage and separation fields (including gas molecules and organic molecules).[11–14] Specific to the adsorption of organic dyes, the highly tuneable pore geometry and chemistry of MOFs could be utilized to regulate the adsorption and separation of dye molecules that feature distinct sizes and characteristics.[15,16]

For the achievement of function targeted structural tuning of MOFs, the rational design of organic ligands is critical.[17] For instance, the metal–ligand bonding affinity could influence the stability of MOFs, the structural flexibility of MOFs could rely on the variable configuration of ligands, and the topology of MOFs is usually determined by the geometry of ligands.[5,13] Aiming at the construction of MOFs for dye adsorption, the stability and porosity structure of framework are two important factors that could determine the performances of the MOFs. In this consideration, the utilization of carboxyl–pyrazole based ligands could be an ideal choice. On the one hand, carboxyl groups possess a variety of coordination modes, providing more possibilities to form novel MOFs in the process of self-assembly.[17,18] On the other hand, based on the hard and soft acids and bases (HSAB) principle, the pyrazole group can form strong bridging interaction with soft Lewis acid metal ions, which has important significance for the stabilization of coordination frameworks.[5,19–21] Furthermore, there are similar characteristics between a carboxyl group and a pyrazole group, including similar electric charges and coordination modes, but subtle coordination ability.[22] Therefore, MOFs feature intriguing and stable architectures and are expected to be constructed with ligands by integrating carboxyl groups with pyrazole groups.[23–26]

Taking all these aspects mentioned above into account and as a continuous work of our group,[14,27] we have proceeded the construction of MOFs based on pyrazole functionalized carboxylic acid ligands for dye adsorption. Herein, two Zn(II) MOFs, $\{(NH_2Me_2)[Zn(Pycia)]\}_n$ (MOF-**1**) and $\{(NH_2Me_2)[Zn_2(Pycia)(PBA)]\}_n$ (MOF-**2**) (H_3Pycia = 5-(1*H*-pyrazole-4-carboxamido)isophthalic acid and H_2PBA = 4-(1*H*-pyrazol-4-yl)benzoic acid), were reported. MOF-**1** exhibits a

[a] *School of Materials Science and Engineering, National Institute for Advanced Materials, Tianjin Key Laboratory of Metal and Molecule-Based Material Chemistry, Nankai University, Tianjin 300350, China. E-mail: mh@nankai.edu.cn, changze@nankai.edu.cn*
[b] *Collaborative Innovation Center of Chemical Science and Engineering (Tianjin), Tianjin 300072, China*
[c] *State Key Laboratory of Structural Chemistry, Fujian Institute of Research on the Structure of Matter, Chinese Academy of Sciences, Fuzhou, Fujian 350002, China*
[d] *State Key Laboratory of Elemento-Organic Chemistry, College of Chemistry, Nankai University, Tianjin 300071, China*

† Electronic supplementary information (ESI) available. CCDC 1986169 and 1986170. For ESI and crystallographic data in CIF or other electronic format see DOI: 10.1039/d0ce00798f

‡ These authors contributed equally to this work.

porous framework with 3,6-connected topology and one-dimensional (1D) channels of about 6.0 Å in diameter. By introducing H_2PBA to the assembly system, MOF-**2** was obtained, which reveals a 3,5-connected topology and an enlarged pore diameter of about 15.0 Å. The result indicates that the mixed-ligand strategy is a promising and convenient method for the tuning of MOF structure. Furthermore, MOF-**1** and MOF-**2** are negatively charged frameworks and possess positive ions in the channels, which exhibit favourable selective adsorption of organic cationic dyes based on charge and size-matching effect (Scheme 1).

Single X-ray diffraction study revealed that MOF-**1** crystallizes in the orthorhombic system with the space group *Pbcn*. The asymmetric unit contains one Zn(II) ion and one $Pycia^{3-}$ ligand (Fig. 1a). According to the charge balance consideration, the anionic framework is balanced by $(NH_2\text{-}Me_2)^+$, from the decomposition of the DMF solvent during the solvothermal reaction. Each Zn(II) ion is coordinated with two O atoms and two N atoms from four $Pycia^{3-}$ ligands, showing a distorted tetrahedral geometry. Two Zn(II) ions are bridged by four N atoms from two $Pycia^{3-}$ ligands to form a dinuclear second building unit (SBU). The dinuclear SBUs are connected by six $Pycia^{3-}$ ligands to form octahedral substructure (Fig. 1e), which are further linked by $Pycia^{3-}$ ligands to generate a three-dimensional (3D) framework (Fig. 1d and f). The network reveals 1D channels with a diameter of 6.0 Å along the *c* axis (Fig. 1d, considering the van der Waals radius). In detail, the 1D channel could be considered as a linear assembly (Fig. 1c) of hexahedral cages in an ABAB⋯arrangement, of which the cages are defined by the ligands and metal centres (Fig. 1b). The accessible volume of the framework is about 66.5% of the cell volume, according to the PLATON[28] analysis after removing all the guest molecules. Furthermore, the framework could be viewed as a (3,6)-connected network with ***apo*** topology with the Schläfli symbol of $\{4{\cdot}6^2\}_2\{4^2{\cdot}6^9{\cdot}8^4\}$, where the SBUs and $Pycia^{3-}$ ligands are simplified as 6-connected and 3-connected nodes, respectively (Fig. S4†).

MOF-**2** crystallizes in the trigonal system with the space group $P3_221$. The asymmetric unit contains two distinct Zn(II) ions, one $Pycia^{3-}$ ligand, and one PBA^{2-} ligand (Fig. 2a). Each Zn(II) ion is coordinated with two N atoms from one $Pycia^{3-}$ and one PBA^{2-} ligands and two O atoms from one $Pycia^{3-}$ and one PBA^{2-} ligands, showing a distorted tetrahedral geometry, which is similar to the Zn(II) ion in MOF-**1**. The two adjacent Zn(II) ions are bonded into a dinuclear SBU with four N atoms from one tritopic $Pycia^{3-}$ and one linear PBA^{2-} ligands, and two O atoms from one PBA^{2-} ligand. The dinuclear SBU as a polyhedral centre is connected by three $Pycia^{3-}$ and two PBA^{2-} ligands to form a trigonal bipyramid (Fig. 2e). The trigonal bipyramids are further connected by

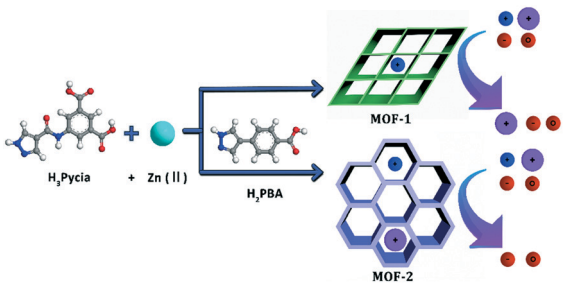

Scheme 1 Schematic representation of the construction of MOF-**1** and MOF-**2** for selective adsorption of organic dyes.

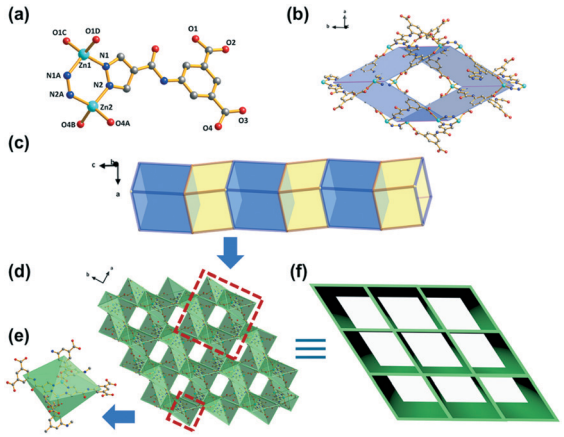

Fig. 1 Crystal structure of MOF-**1**: (a) coordination environment of Zn(II) ions and $Pycia^{3-}$ ligands; (b) the hexahedral cage defined by dinuclear SBUs and $Pycia^{3-}$ ligands; (c) one dimensional channel assembled by the hexahedral cages along the *c* axis; (d) the 3D framework with one dimensional channels; (e) the octahedral representation of the dinuclear SBU; (f) schematic illustration of the 3D framework of MOF-**1** with one dimensional channels.

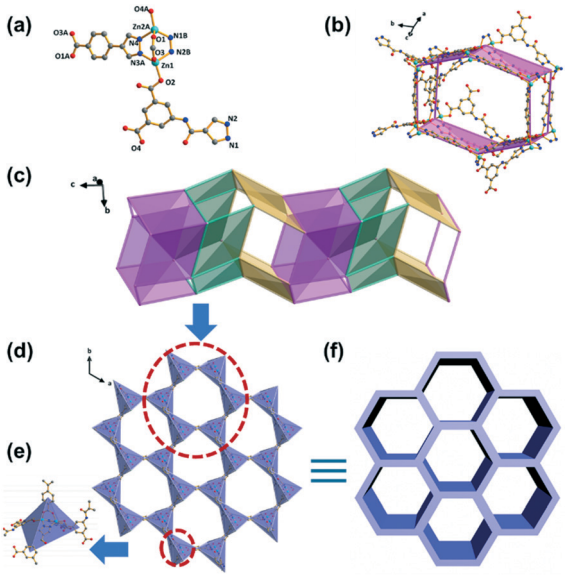

Fig. 2 Crystal structure of MOF-**2**: (a) coordination environment of Zn(II) ions and ligands; (b) the hexagonal prism cage formed by dinuclear SBUs and $Pycia^{3-}$ and PBA^{2-} ligands; (c) the one dimensional channel formed by the hexagonal prism cages along the *c* direction; (d) the 3D framework with one dimensional channels; (e) the trigonal bipyramidal representation of dinuclear SBU; (f) schematic illustration of the 3D framework of MOF-**2** with one dimensional channels.

the ligands to form a three-dimensional framework with 1D hexagonal channels (Fig. 2d and f), of which the aperture is about 15 Å (considering the van der Waals radius), larger than that of MOF-**1**. Meanwhile, twelve dinuclear SBUs as vertices form a hexagonal prism cage (Fig. 2b), then three cages at different angles as the minimum repeated unit construct a 1D channel along the *c* axis (as shown in Fig. 2c). The anionic framework is charge balanced by $(NH_2Me_2)^+$. For the 3D framework, the effective free volume is 80.6% of the cell volume, which is much higher than that of MOF-**1**. In addition, the topological analysis of the framework results in a (3,5)-connected new network with the Schläfli symbol of $\{4{\cdot}5^2\}\{4{\cdot}5^3{\cdot}6^2{\cdot}7^3{\cdot}8\}$, where the SBUs and $Pycia^{3-}$ ligands are simplified as 5-connected and 3-connected nodes, respectively (Fig. S5†).

By comparing the structural characteristics of the two MOFs, it is obvious that the introduction of the auxiliary H_2PBA ligand tunes the structure of the MOF effectively. The Zn(II) ions in the two compounds reveal similar coordination modes and the pyrazole groups in the two kinds of the ligands adopt the same coordination modes. However, the carboxyl groups in PBA^{2-} ligand adopt a bidentate bridging mode to connect the adjacent Zn(II) ions to form the dinuclear SBU, while $Pycia^{3-}$ ligand takes a monodentate bridging mode to link one Zn (II) ion. Obviously, the PBA^{2-} ligand as a spacer could further increase the distance between the inorganic SBUs to result in a more accessible pore volume. As a result, the channels of MOF-**1** are formed by the hexahedral cages, while the channels of MOF-**2** are constructed by the hexagonal prism cages with larger apertures. In consideration of the dye adsorption application, the larger pore volume and aperture could benefit the adsorption of organic molecules with larger backbone of dyes and improve adsorption capacity.

Before the investigation of their dye adsorption properties, the phase purity and thermal stabilities of MOF-**1** and MOF-**2** were characterized by powder X-ray diffraction (PXRD) and thermogravimetric (TG) analyses (Fig. S6–S9†). As shown in Fig. S6 and S7,† the well-matched experimental and simulated XRD patterns indicate the high phase purity of the bulk samples. The TG profiles show that the frameworks of MOF-**1** and MOF-**2** could be stable up to 350 °C (Fig. S8 and S9†).

Since the frameworks of MOF-**1** and MOF-**2** are anionic, they are suitable for the adsorption of cationic dyes. Accordingly, two sets of experiments were designed to evaluate their dye adsorption behaviours. The first group focused on dyes with similar sizes, but different charges (including methylene blue: MB^+, thiazole orange: TO^+, sudan I: SD^0, coumarin: CM^0, methyl orange: MO^-, and lllion chrome blue and black: LB^-). Based on the experimental results of the first group, the second group concentrated on cationic dyes with different sizes (such as methylene blue: MB^+, thiazole orange: TO^+, rhodamine 6G: $R6G^+$, and victoria blue: VB^+) (Fig. S10†).

For the first set of experiments, the cationic dye solutions containing MB^+ (20 mg L^{-1}) and TO^+ (20 mg L^{-1}) have gradually faded during 24 hours when 10 mg of MOF-**1** and MOF-**2** was added. Accordingly, the colorless crystals turned into blue and orange in the solution of MB^+ and TO^+, respectively. On the contrary, the colors of anionic solutions containing MO^- (20 mg L^{-1}) and AR^- (20 mg L^{-1}) and electrically neutral solutions containing SD^0 (20 mg L^{-1}) and CM^0 (20 mg L^{-1}) remained. The phenomenon coincided with the measurement results by UV-vis spectroscopy (Fig. S11 and S12†). The effective adsorption of cationic molecules could be attributed to the ionic interaction between anionic frameworks and the cationic dye molecules. Moreover, the $(NH_2Me_2)^+$ guests in the channels could be readily exchanged with cationic dyes to promote the adsorption of dyes.

Furthermore, to verify the adsorption selectivity of MOF-**1** and MOF-**2** toward cationic dyes, competitive experiments were performed in the presence of different anionic or neutral dyes. The mixed solutions (20 mg L^{-1}, 1 : 1 by volume ratio) including MB^+/SD^0, MB^+/CM^0, MB^+/MO^-, and MB^+/LB^- (Fig. S13† for MOF-**1** and Fig. S15† for MOF-**2**) and TO^+/SD^0, TO^+/CM^0, TO^+/MO^-, and TO^+/LB^- (Fig. S14† for MOF-**1** and Fig. S16† for MOF-**2**) were utilized for the experiments, and the results showed that the two MOFs could selectively adsorb MB^+ and TO^+. All the results demonstrate that MOF-**1** and MOF-**2** are not only high-efficiency porous materials for the adsorption of MB^+ and TO^+, but also that their adsorption behaviours are not interfered by other anionic or neutral dyes.

In consideration of the distinctive pore dimensions of MOF-**1** and MOF-**2**, their adsorption selectivity to cationic dyes with different sizes was also investigated with $R6G^+$ and

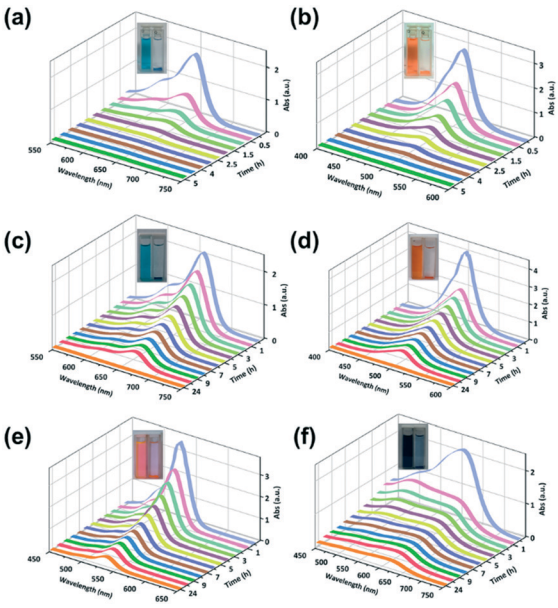

Fig. 3 UV-vis spectra of MB^+ solutions (a) and TO^+ solutions (b) upon adsorption by MOF-**1**; UV-vis spectra of MB^+ solutions (c), TO^+ solutions (d), $R6G^+$ solutions (e) and VB^+ solutions (f) upon adsorption by MOF-**2**.

VB^+, which reveal a much larger molecular backbone than that of MB^+ and TO^+ (Fig. S10†). As revealed by the UV-vis spectroscopy data (Fig. S11†), when MOF-**1** was added into the dye solution (20 mg L^{-1}), the concentration of MB^+ and TO^+ dropped quickly (Fig. 3a and b), while the concentration of $R6G^+$ and VB^+ remained nearly unchanged. In contrast, for MOF-**2**, all four kinds of dyes could be removed from the solution effectively (Fig. 3c–f). The distinctive dye adsorption behaviours of MOF-**1** and MOF-**2** toward dye molecules with different sizes are well consistent with their structures. The enlarged pore aperture of MOF-**2** allows the adsorption of dyes with larger dimension, while the limited pore size of MOF-**1** results in its size selective adsorption toward smaller dyes.

In addition, the adsorption capacities of MOF-**1** and MOF-**2** toward MB^+ and TO^+ were determined to further evaluate the effectiveness of the mixed-ligand strategy for dye adsorption optimization. As shown in Fig. S18,† for both MOF-**1** and MOF-**2**, the equilibrium adsorption amount (q_e) reaches a plateau with increasing initial concentration of the adsorbent (c_0) in the q_e–c_0 profile for both MB^+ and TO^+. The adsorption capacity of MB^+ reaches 29 mg g^{-1} for MOF-**1** and 87 mg g^{-1} for MOF-**2**, respectively. As for TO^+, the capacities are about 13 mg g^{-1} and 76 mg g^{-1} for MOF-**1** and MOF-**2**, respectively. It is clearly evidenced that the MOF-**2** owning the enlarged pore dimension and pore volume has an improved adsorption capacity relative to MOF-**1**. By comparing with the dye adsorption performances reported in relative research,[29–32] the distinct dye selectivity and capacity of MOF-**1** and MOF-**2** further verify the importance of charge effect as well as the size-matching effect factors for performance optimization. All these results demonstrated that mixed-ligand strategy is a promising method for structural tuning and optimizing properties of MOFs.

In summary, two Zn(II) MOFs with a distinct architecture have been constructed with trigonal H_3Pycia and linear H_2PBA ligands. Compared with MOF-**1** possessing hexahedral cages, MOF-**2** exhibits a structure with larger hexagonal prism cages resulting from the existence of auxiliary H_2PBA ligand. Based on charge and size-matching effect, they exhibit size selective adsorption behaviour for cationic organic dyes. Therefore, two MOFs could be considered as the promising materials to clean environment by the simple physical adsorption of organic dyes.

Conflicts of interest

There are no conflicts to declare.

Acknowledgements

This work was supported by the NSFC (21531005, 21875115, and 21671112) and the Programme of Introducing Talents of Discipline to Universities (B18030).

Notes and references

1 A. Khatri, M. H. Peerzada, M. Mohsin and M. White, *J. Cleaner Prod.*, 2015, **87**, 50–57.
2 X. Li, Y. X. Liu, J. Wang, J. Gascon, J. S. Li and B. Van der Bruggen, *Chem. Soc. Rev.*, 2017, **46**, 7124–7144.
3 M. Mon, R. Bruno, J. Ferrando-Soria, D. Armentano and E. Pardo, *J. Mater. Chem. A*, 2018, **6**, 4912–4947.
4 V. K. Gupta and Suhas, *J. Environ. Manage.*, 2009, **90**, 2313–2342.
5 S. Yuan, L. Feng, K. C. Wang, J. D. Pang, M. Bosch, C. Lollar, Y. J. Sun, J. S. Qin, X. Y. Yang, P. Zhang, Q. Wang, L. F. Zou, Y. M. Zhang, L. L. Zhang, Y. Fang, J. L. Li and H. C. Zhou, *Adv. Mater.*, 2018, **30**, 1704303.
6 Q. G. Zhai, X. H. Bu, X. Zhao, D. S. Li and P. Y. Feng, *Acc. Chem. Res.*, 2017, **50**, 407–417.
7 S. Dang, Q. L. Zhu and Q. Xu, *Nat. Rev. Mater.*, 2018, **3**, 17075.
8 M. J. Kalmutzki, N. Hanikel and O. M. Yaghi, *Sci. Adv.*, 2018, **4**, eaat9180.
9 H. C. Zhou and S. Kitagawa, *Chem. Soc. Rev.*, 2014, **43**, 5415–5418.
10 S. Dissegna, K. Epp, W. R. Heinz, G. Kieslich and R. A. Fischer, *Adv. Mater.*, 2018, **30**, 1704501.
11 K. Adil, Y. Belmabkhout, R. S. Pillai, A. Cadiau, P. M. Bhatt, A. H. Assen, G. Maurin and M. Eddaoudi, *Chem. Soc. Rev.*, 2017, **46**, 3402–3430.
12 D. X. Xue, Q. Wang and J. F. Bai, *Coord. Chem. Rev.*, 2019, **378**, 2–16.
13 W. Lu, Z. Wei, Z.-Y. Gu, T.-F. Liu, J. Park, J. Park, J. Tian, M. Zhang, Q. Zhang, T. Gentle Iii, M. Bosch and H.-C. Zhou, *Chem. Soc. Rev.*, 2014, **43**, 5561–5593.
14 Y.-Y. Jia, X.-T. Liu, R. Feng, S.-Y. Zhang, P. Zhang, Y.-B. He, Y.-H. Zhang and X.-H. Bu, *Cryst. Growth Des.*, 2017, **17**, 2584–2588.
15 Y. Li, Z. Yang, Y. Wang, Z. Bai, T. Zheng, X. Dai, S. Liu, D. Gui, W. Liu, M. Chen, L. Chen, J. Diwu, L. Zhu, R. Zhou, Z. Chai, T. E. Albrecht-Schmitt and S. Wang, *Nat. Commun.*, 2017, **8**, 1354.
16 Y. C. He, J. Yang, W. Q. Kan, H. M. Zhang, Y. Y. Liu and J. F. Ma, *J. Mater. Chem. A*, 2015, **3**, 1675–1681.
17 A. Kirchon, L. Feng, H. F. Drake, E. A. Joseph and H. C. Zhou, *Chem. Soc. Rev.*, 2018, **47**, 8611–8638.
18 J. Zhang, F. Li and Q. Sun, *Appl. Surf. Sci.*, 2018, **440**, 1219–1226.
19 G. N. Liu, M. J. Zhang, W. Q. Liu, H. Sun, X. Y. Li, K. Li, C. Z. Ren, Z. W. Zhang and C. Li, *Dalton Trans.*, 2015, **44**, 18882–18892.
20 Y.-S. Luo, J.-L. Chen, X.-H. Zeng, L. Qiu, L.-H. He, S.-J. Liu and H.-R. Wen, *Chin. Chem. Lett.*, 2017, **28**, 1027–1030.
21 V. Colombo, S. Galli, H. J. Choi, G. D. Han, A. Maspero, G. Palmisano, N. Masciocchi and J. R. Long, *Chem. Sci.*, 2011, **2**, 1311–1319.
22 D. J. Tranchemontagne, K. S. Park, H. Furukawa, J. Eckert, C. B. Knobler and O. M. Yaghi, *J. Phys. Chem. C*, 2012, **116**, 13143–13151.

23 F. Y. Yi, J. P. Li, D. Wu and Z. M. Sun, *Chem. – Eur. J.*, 2015, **21**, 11475–11482.
24 L.-L. Han, X.-Y. Zhang, J.-S. Chen, Z.-H. Li, D.-F. Sun, X.-P. Wang and D. Sun, *Cryst. Growth Des.*, 2014, **14**, 2230–2239.
25 L.-L. Han, T.-P. Hu, K. Mei, Z.-M. Guo, C. Yin, Y.-X. Wang, J. Zheng, X.-P. Wang and D. Sun, *Dalton Trans.*, 2015, **44**, 6052–6061.
26 L.-L. Han, S.-N. Wang, Z. Jagličić, S.-Y. Zeng, J. Zheng, Z.-H. Li, J.-S. Chen and D. Sun, *CrystEngComm*, 2015, **17**, 1405–1415.
27 X.-T. Liu, Y.-Y. Jia, Y.-H. Zhang, G.-J. Ren, R. Feng, S.-Y. Zhang, M. J. Zaworotkoc and X.-H. Bu, *Inorg. Chem. Front.*, 2016, **3**, 1510–1515.
28 A. L. Spek, *J. Appl. Crystallogr.*, 2003, **36**, 7–13.
29 Mantasha I., M. Shahid, H. A. M. Saleh, K. M. A. Qasem and M. Ahmad, *CrystEngComm*, 2020, **22**, 3891–3909.
30 L. Lu, J. Wu, J. Wang, J.-Q. Liu, B.-H. Li, A. Singh, A. Kumar and S. R. Batten, *CrystEngComm*, 2017, **19**, 7057–7067.
31 Y.-F. Hui, C.-L. Kang, T. Tian, S. Dang, J. Ai, C. Liu, H.-R. Tian, Z.-M. Sun and C.-Y. Gao, *CrystEngComm*, 2017, **19**, 1564–1570.
32 X. Zhang, Y. Gao, H. Liu and Z. Liu, *CrystEngComm*, 2015, **17**, 6037–6043.